# Positron Emission Mammography–Guided Breast Biopsy

Raymond R. Raylman, Stan Majewski, Andrew G. Weisenberger, Vladimir Popov, Randy Wojcik, Brian Kross, Judith S. Schreiman, and Harry A. Bishop

*Center for Advanced Imaging, Department of Radiology, West Virginia University, Morgantown, West Virginia; and Detector Group, Jefferson Laboratory, Newport News, Virginia*

Positron emission mammography (PEM) is a technique to obtain planar images of the breast for detection of potentially cancerous, radiotracer-avid tumors. To increase the diagnostic accuracy of this method, use of minimally invasive methods (e.g., core biopsy) may be desirable for obtaining tissue samples from lesions detected with PEM. The purpose of this study was to test the capabilities of a novel method for performing PEM-guided stereotactic breast biopsies. **Methods:** The PEM system consisted of 2 square (10 × 10 cm) arrays of discrete scintillator crystals. The detectors were mounted on a stereotactic biopsy table. The stereotactic technique used 2 PEM images acquired at ±15° and a new trigonometric algorithm. The accuracy and precision of the guidance method was tested by placement of small point sources of $^{18}$F at known locations within the field of view of the imager. The calculated positions of the sources were compared with the known locations. In addition, simulated stereotactic biopsies of a breast phantom consisting of a 10-mm-diameter gelatin sphere containing a concentration of $^{18}$F-FDG consistent with that reported for breast cancer were performed. The simulated lesion was embedded in a 4-cm-thick slab of gelatin containing a commonly reported concentration of FDG, simulating a compressed breast (target-to-background ratio, approximately 8.5:1). An anthropomorphic torso phantom was used to simulate tracer uptake in the organs of a patient 1 h after a 370-MBq injection of FDG. Five trials of the biopsy procedure were performed to assess repeatability. Finally, a method for verifying needle positioning was tested. **Results:** The positions of the point sources were successfully calculated to within 0.6 mm of their true positions with a mean error of ±0.4 mm. The biopsy procedures, including the method for verification of needle position, were successful in all 5 trials in acquiring samples from the simulated lesions. **Conclusion:** The success of this new technique shows its potential for guiding the biopsy of breast lesions optimally detected with PEM.

**Key Words:** breast biopsy; positron emission mammography; radionuclide guidance

**J Nucl Med 2001; 42:960–966**

Several groups have constructed dedicated, compact, high-resolution, high-sensitivity planar breast imagers for use with positron-emitting radiopharmaceuticals, such as $^{18}$F-FDG (*1–3*). The improved imaging performance of these specialized breast-imaging devices, called positron emission mammography (PEM) scanners, means that they can potentially be effective in detecting small breast lesions. Additionally, the often-excellent specificity of FDG can allow a more selective application of subsequent confirming diagnostic procedures (e.g., percutaneous core biopsy) in cystic breasts, where multiple benign lesions can be present along with malignant tumors, or in radiographically dense breasts, where x-ray mammography can often be suboptimal. The imaging of FDG with PET has not shown sufficient specificity to justify use as a sole means for evaluation of suggestive breast lesions. Ultimately, final diagnoses of breast cancer should be based on information gained by acquisition and analysis of tumor tissue samples obtained through either percutaneous core or surgical biopsies.

Although a biopsy method for use with another specialized breast-imaging technique ($^{99m}$Tc-sestamibi scintimammography) has been proposed (*4*), no efficient and accurate method currently exists for the stereotactic biopsy of breast lesions using PEM images. The use of PEM in conjunction with x-ray mammography has, however, been proposed for guiding biopsy (*3*). This method relies on the use of a standard stereotactic x-ray mammogram–based system to calculate the position of suggestive lesions also detected with PEM. This reliance on the ability to detect the lesion with x-rays may limit the versatility of the technique. Specifically, the dual-imaging method may be suboptimal in situations in which PEM imaging indicates a suggestive lesion but standard x-ray mammography yields indeterminate results because of cystic or radiodense breast tissue (*5–8*). To address this problem, we have taken a previously proposed method for calculating the stereotactic coordinates of photon-emitting objects (*9*) and adapted it to the guidance of breast biopsy using PEM images. The goal of this study was to explore the capabilities of this new technique for guiding the biopsy of suggestive radiotracer-avid breast lesions.

Received May 18, 2000; revision accepted Nov. 17, 2000.

For correspondence or reprints contact: Raymond R. Raylman, PhD, Health Sciences Center South, West Virginia University, Radiology/PET Box 9236, Morgantown, WV 26506-9236.

## MATERIALS AND METHODS

### PEM Imager

The PEM system comprised 2 separate, opposing coincidence detector units, each consisting of a 4 × 4 square array of compact R5900-C8 position-sensitive photomultiplier tubes (PSPMT) (Hamamatsu Photonics K.K., Hamamatsu, Japan). The new flangeless version of this photomultiplier, with a 22-mm-square photocathode size, permitted tight arrangement of the PSPMTs. Two arrays of 900 (30 × 30) gadolinium oxy-orthosilicate (GSO) scintillator crystals (Hitachi Chemical Co., Ltd., Tokyo, Japan) were used to construct the PEM detector heads. Each GSO crystal measured 3.1 × 3.1 × 10 mm. The sides of the crystals facing the PSPMT windows were polished; all other surfaces had a rough-cut finish. The crystals were individually wrapped with white Teflon (DuPont, Wilmington, DE) tape to optically separate individual pixels and to improve light collection through diffusive reflection. The crystal arrays were held in place with nylon mounting frames. Because of the thickness of the Teflon tape, the average pixel spacing was 3.3 mm. The scintillator arrays were coupled to the PSPMT arrays through 1-cm-thick acrylic light diffusers. Contact of the scintillator arrays with the diffusers and contact of the diffusers with the PSPMT arrays were maintained with the nylon support frames. To minimize resolution loss, we did not use coupling grease (*10*). The detector heads were mounted 56 cm apart on a breast biopsy apparatus (Lorad, Danbury, CT). The PEM biopsy imager had a 10 × 10 cm field of view, which was significantly larger than the 5 × 5 cm field of view of the x-ray mammography unit of the Lorad system.

Each PSPMT had its own voltage divider, providing voltage distribution to normalize signal gains. Readout of the PSPMT arrays (each PSPMT having 8 [4(X) + 4(Y)] output anode wires) was simplified by interconnecting corresponding X and Y wires from different PSPMTs to form 16(X) × 16(Y) combined anode outputs. Each combined X and Y output was amplified by custom amplifier boards located in the detector heads before being processed in a mini CAMAC crate (LeCroy Corp., Chestnut Ridge, NY) by 2 analog-to-digital converters (ADCs) (4300B fast encoding and readout ADC; LeCroy Corp.). The last dynodes of all the PSPMTs were connected to provide a common 300-ns-wide trigger pulse to the ADCs. A 10-ns coincidence window was used to reduce acceptance of random coincidence events. Data acquisition was controlled with software written using the Kmax environment (Sparrow, Inc., Starkville, MS) resident on a Power Macintosh G3 personal computer (Apple Computer, Inc., Cupertino, CA). The bodies of the detector heads were constructed from tungsten plates 3.175 mm (0.125 in.) thick to shield the scintillators from photon flux originating in a patient. The addition of this shielding and the use of high-speed electronics helped further reduce the acceptance of random coincidence events and minimized detector dead time while introducing minimal dead space between the detector array and the patient. Random coincidence events were monitored using a delayed-coincidence method for offline correction of the PEM images.

A truncated center-of-gravity algorithm (*11*) was used to maximize crystal–pixel identification in the raw image. Events were positioned using lookup-table crystal maps calculated for each detector unit. An energy discrimination window (400–600 keV) was applied to data from each pixel to reduce acceptance of Compton scatter events. Planar images were produced using a confocal reconstruction algorithm similar to the weighted-back-projection method used by Thompson et al. (*1*). Seven image planes were reconstructed: the central focal plane and the planes ±1 cm, ±2 cm, and ±3 cm from the central focal plane. The intrinsic resolution of the imager was 3.9 mm.

### Stereotactic Method

The calculation of stereotactic coordinates was based on a method proposed by Raylman et al. (*9*). This approach relies on the fact that the position of a photon-emitting object in the scanner coordinate system (R and $\phi$) is transformed by the imaging process into the sinogram coordinate frame (L and $\theta$). This transformation is expressed by the equation:

$$L = R \times \sin(\phi - \theta). \quad \text{Eq. 1}$$

L is the distance from the center of the detector array to the position of the line integral of photons detected from the object, R is the distance from the object to the center of the scanner, $\phi$ is the angular position of the object in the scanner, and $\theta$ is the angular position of the detector array. When images are acquired at discrete view angles of $\theta = 0°$ and $\gamma$, Equation 1 can be rewritten as:

$$L_1 = R \times \sin\phi; [\theta = 0°] \quad \text{Eq. 2}$$

and

$$L_2 = R \times \sin(\phi - \theta) = R \times [(\sin\phi \times \cos\gamma) - (\cos\phi \times \sin\gamma)]; [\theta = \gamma]. \quad \text{Eq. 3}$$

$L_1$ is the distance from the line integral sampling the photon flux from the object to the center of the detector arrays positioned at a rotation angle $\theta = 0°$. $L_2$ is the distance from the line integral to the center of the PEM detectors at a detector rotation angle $\theta = \gamma$. Equation 3 was cast into a more useful form by insertion of the trigonometric identity for $\sin(\phi - \gamma)$. Dividing Equation 3 by Equation 2, we obtain the relationship:

$$\frac{L_2}{L_1} = \cos\gamma - \cos\phi \times \sin\gamma. \quad \text{Eq. 4}$$

The position of an object in the scanner was calculated by measuring the distances $L_1$ and $L_2$ from PEM images acquired at 2 different view angles. Next, given the angle $\gamma$, Equation 4 was solved for the angular position of the object in the imager ($\phi$). The distance between the object and the center of the PEM imager (R) was then calculated using Equation 2. The *x*-coordinate (horizontal position) and *z*-coordinate (depth) of the object in the imager reference frame were given by $x = R \times \sin\phi$ and $z = R \times \cos\phi$.

Because the Lorad system was designed to acquire images at ±15°, not 0° and some angle $\gamma$, coordinates had to be transformed to obtain the position of objects in the scanner reference frame. The distance $L_1$ was measured using the PEM image acquired at −15°, and $L_2$ was measured using the +15° image. The image acquired at −15° was defined as the 0° view in the algorithm coordinate frame. This coordinate system was thus rotated by −15° relative to the Lorad coordinate system. Therefore, the *x*- and *z*-coordinates calculated using the algorithm had to be rotated by +15° to obtain the position of the object in the *x*–*z* plane of the Lorad apparatus. For this apparatus, which acquires images at ±15°, the angle $\gamma$ in Equation 4 was 30°. The *y*-coordinate (vertical position) was determined by first locating the detector plane that sampled the center of the object and then, given the spacing between detectors, calculating the distance from the center

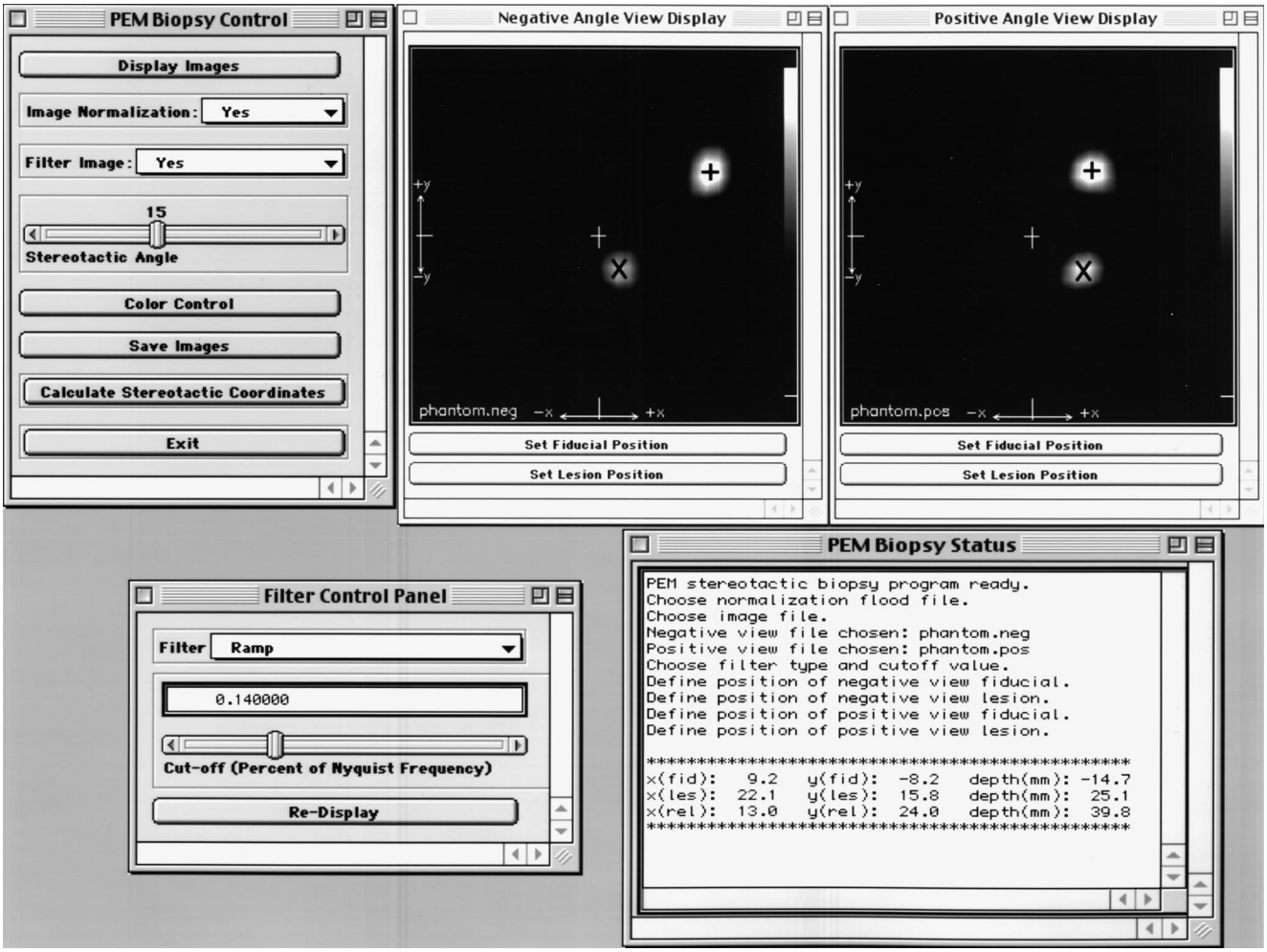


**FIGURE 1.** Stereotactic software user interface. Display windows show ±15° images of breast phantom. User marks center of fiducial marker with × and center of lesion with +.

of the imager to the object. The *y*-coordinate did not have to be transformed.

### User Interface

PEM images were processed using specially developed software created with the Interactive Data Language (IDL) (Research Systems, Inc., Boulder, CO). The user interface is shown in Figure 1. The software allowed the user to change color tables, adjust image brightness, and apply different frequency window functions (ramp, Hanning, or Shepp-Logan filters) to the images to enhance lesion contrast. To account for possible variations in detector performance, the user had the option of applying a normalization procedure. Images were normalized by a pixel-by-pixel multiplication of the image matrices with a matrix of normalization factors calculated using a previously acquired, high-count image of a planar flood source.

The most important function of the software was calculation of stereotactic coordinates. The 2 images (positive- and negative-angle views) were displayed in individual windows. The center of the image of the object in each view was determined by the user and marked using a mouse-driven cursor (Fig. 1). The parameters $L_1$ and $L_2$ necessary for calculation of the stereotactic coordinates were measured from these marked positions. The 3-dimensional coordinates of the object were then calculated and displayed.

### Test of Stereotactic Coordinate Calculation

The accuracy and precision of the stereotactic method were evaluated by positioning point sources, created by soaking 1-mm-diameter alumina silicate beads (Fisher Scientific International, Inc., Hampton, NH) in $^{18}$F, at 5 known locations within the field of view of the scanner using a computer-controlled, 3-axis stage. Images of the sources were acquired at ±15°. From these images, the absolute positions of the point sources in the coordinate frame of the biopsy apparatus were calculated using the technique previously described. The marking of the source positions and calculation of the coordinates were repeated 5 times for each source position to evaluate the precision of the method. The mean calculated values were plotted as a function of the known positions.

### Simulated Stereotactic Breast Biopsy

A series of simulated stereotactic breast biopsies was performed using gelatin breast phantoms consisting of simulated FDG-avid lesions (10-mm-diameter spheres) embedded in 4-cm-thick blocks of gelatin (simulating compressed breasts). The concentration of FDG in the spheres (20.35 kBq/mL) and gelatin blocks simulating normal breast tissue (2.4 kBq/mL) was representative of that reported in human studies 1 h after injection of 370 MBq FDG (*12,13*). The target-to-background concentration ratio was approximately 8.5:1. Food coloring was added to the gelatin used to make

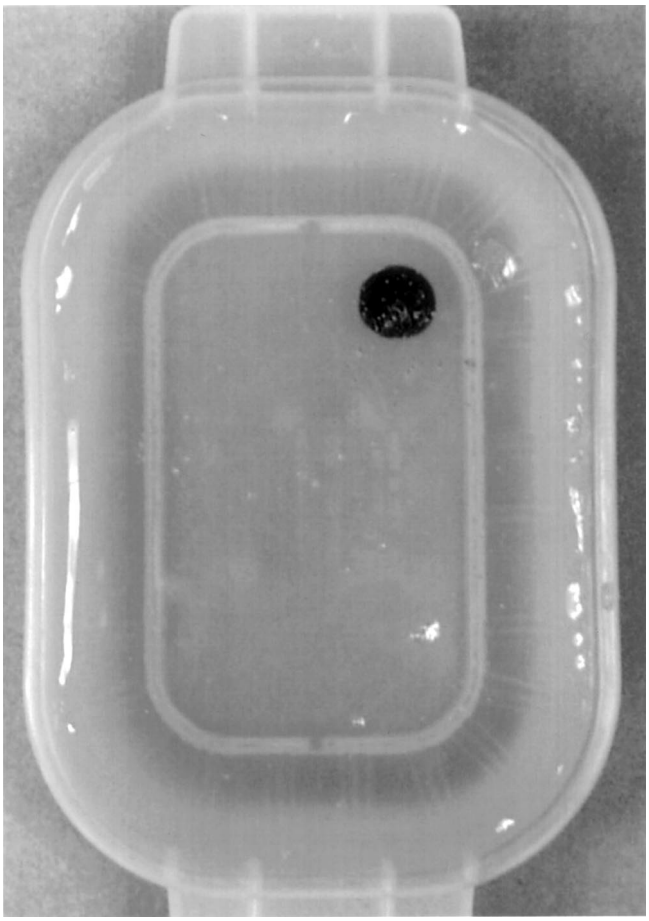

**FIGURE 2.** Gelatin compressed-breast phantom containing 10-mm-diameter simulated lesion.

the spheres so that they could be distinguished from the blocks of gelatin (Fig. 2). The phantom was mounted in the compression plates of the biopsy system. A single 12-mm-diameter hollow acrylic sphere containing liquid with approximately the same concentration of FDG as was in the simulated lesion was attached to the outer surface of the proximal compression plate and used as a fiducial marker for needle placement. Uptake of FDG in a patient was simulated by filling the organs of an anthropomorphic torso phantom (Data Spectrum Corp., Hillsborough, NC) with concentrations of FDG consistent with those measured 1 h after injection of 370 MBq FDG. Simulated liver, adipose, and myocardial tissue concentrations of FDG were 7.1, 3.1, and 7.5 kBq/mL, respectively (*12*,*14*). FDG uptake in the brain and bladder was simulated with a 20-cm-diameter flood phantom and a 500-mL beaker of water containing 37 and 9 MBq, respectively, of $^{18}$F (*12*,*14*). Figure 3 shows the apparatus.

Before PEM imaging, an x-ray mammogram of the breast phantom was acquired at the 0° position. PEM images (240-s acquisition) were then acquired at 0° and ±15°. The stereotactic coordinates of the simulated lesion relative to the fiducial marker were calculated using the ±15° images. The tip of a 14-gauge core biopsy needle (Magnum; Bard Urological Division, Covington, GA) mounted in a spring-loaded biopsy gun (BIP; Bard Urological Division) was positioned at the calculated *x*-, *y*-, and *z*-coordinates. To confirm proper positioning of the needle, we needed to develop a method for verifying needle location. A capillary tube (inner diameter, 0.22 mm; outer diameter, 1.14 mm) containing a small amount of concentrated FDG (185 MBq/mL) was temporarily fixed inside the tip of the biopsy needle so that the biopsy needle could be visualized with the PEM imager. After placement of the needle at the location calculated using the initial set of PEM images, a second set of images was acquired to assess the position of the needle relative to the simulated lesion. After verification of proper needle position, the capillary tube was replaced with the inner stylus of the biopsy needle. The biopsy gun was fired and the gelatin sample removed.

## RESULTS

The plots in Figure 4 show results from the stereotactic coordinate calculations plotted as a function of the known positions of the point sources. The maximum deviation for any single measurement from the known position was 0.6

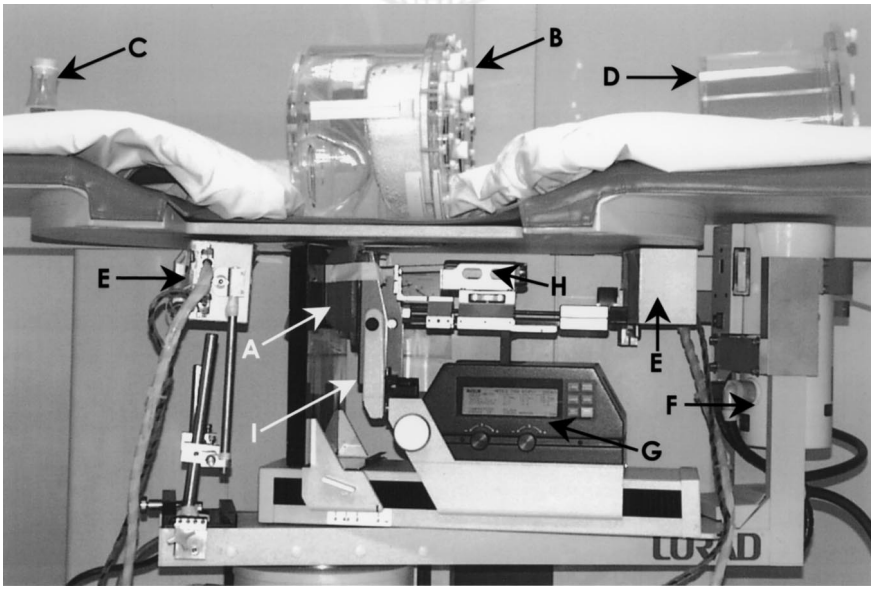


**FIGURE 3.** Experimental setup. Most notable sections of apparatus have been labeled: gelatin breast phantom (A), anthropomorphic torso phantom (B), 500-mL beaker simulating bladder (C), 20-cm-diameter flood phantom simulating brain (D), 2 PEM detector units (E), x-ray tube of breast biopsy apparatus (Lorad, Danbury, CT) (F), biopsy needle positioning unit (G), biopsy gun (H), and proximal compression plate (I).

mm; the mean error was ±0.4 mm. Figure 5A shows the x-ray mammogram of the breast phantom. Figure 5B shows the PEM image of the same phantom. Unlike the x-ray mammogram, the 10-mm-diameter sphere was detectable in the PEM image. The fiducial marker was not in the field of view of the x-ray imager and thus was not detected on the x-ray mammogram. Figure 6 shows an image (−15° view) used to assess needle positioning before firing. All 5 of the core biopsies of the simulated breasts successfully extracted samples (as determined by the color of the gelatin removed by the biopsy needle) from the spheres. During image

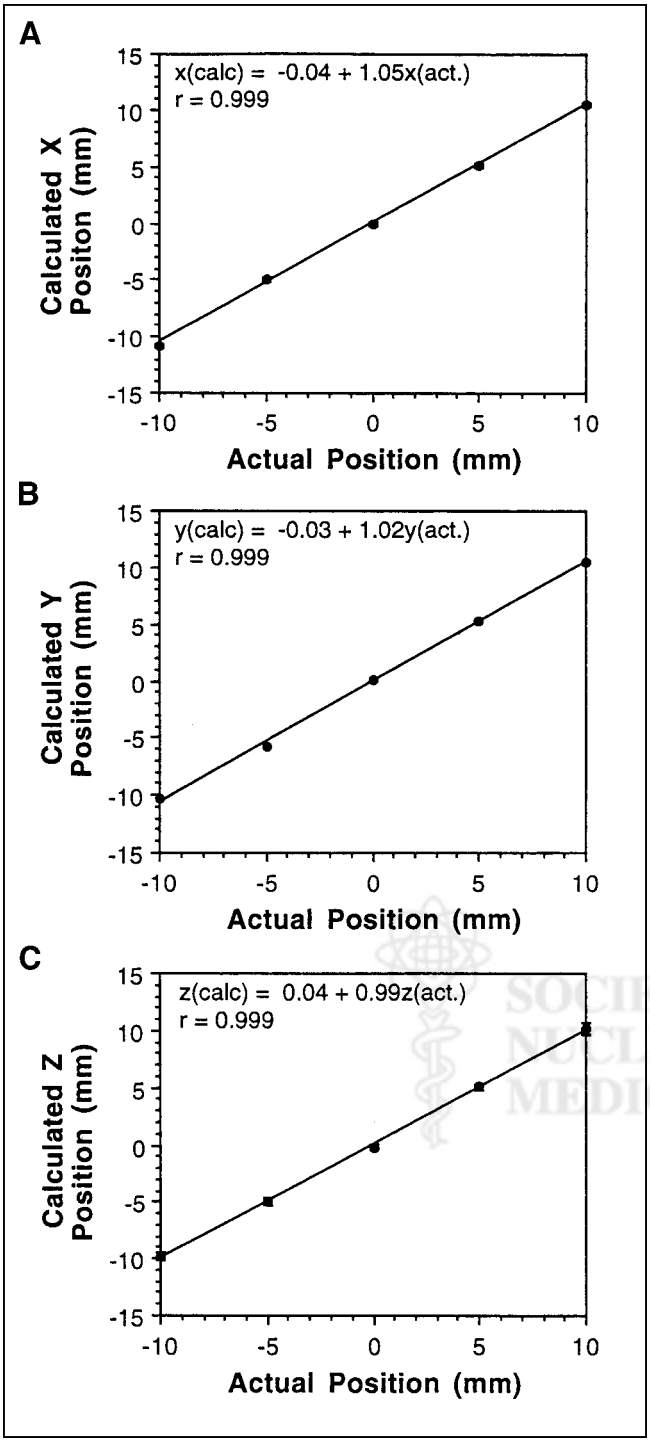


**FIGURE 4.** Plots of calculated versus known positions of $^{18}F$ point sources show results for *x*-coordinate (A), *y*-coordinate (B), and *z*-coordinate (C). Fits of each set of data to straight line are also shown.

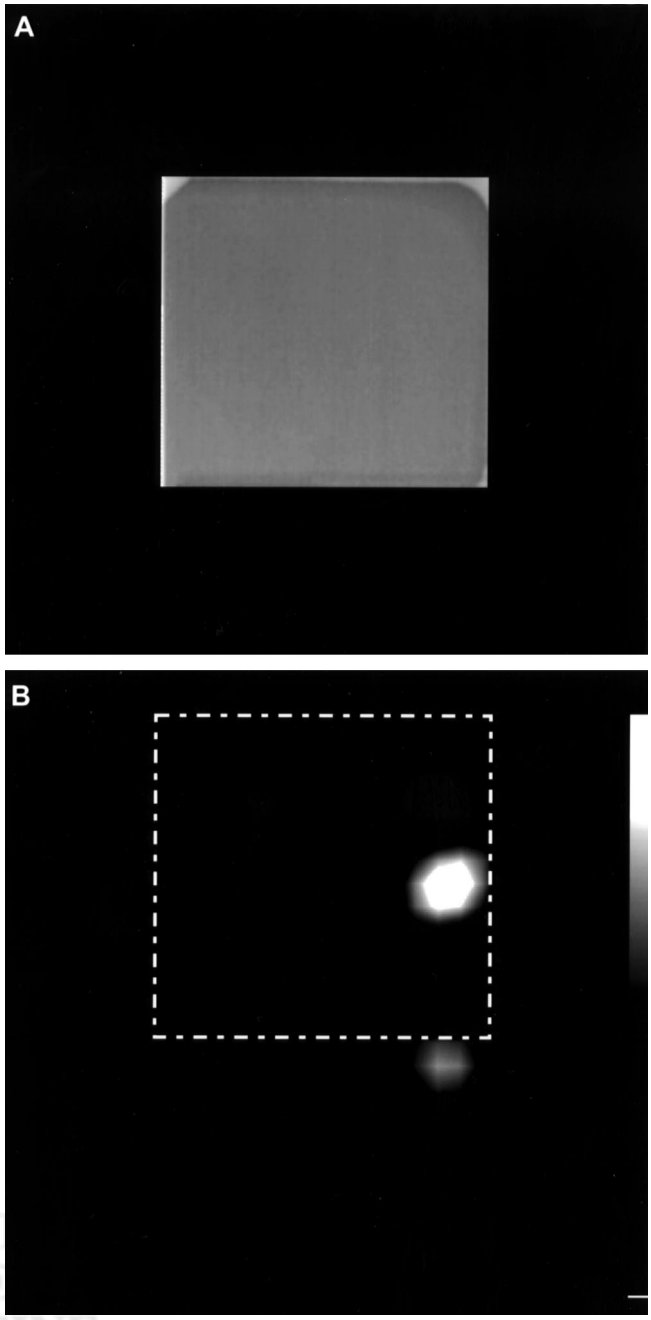


**FIGURE 5.** Images of gelatin breast phantom. (A) X-ray mammogram of phantom acquired at 0°. (B) PEM image of phantom acquired at 0°. Dashed box delineates outline of field of view of x-ray mammography unit. Ramp filter window function with cutoff value of 14% of Nyquist frequency was applied to image. Object in lower portion of PEM image is fiducial marker. Size scales of x-ray mammogram and PEM image are same to show differences in field of view of the 2 imagers.

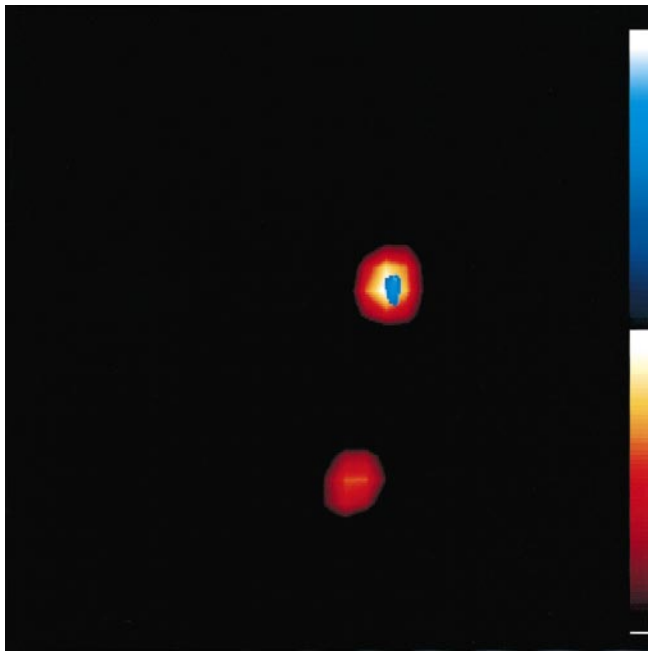

**FIGURE 6.** Image of biopsy needle tip (blue color scale) overlaid with filtered PEM image of breast phantom (red color scale) used to assess needle positioning before firing of biopsy gun. Ramp filter window function with cutoff value of 14% of Nyquist frequency was applied to image. Image was acquired at detector rotation angle of −15°.

acquisition, the single-event rate in each PEM detector head was approximately 750 kcps.

## DISCUSSION

The use of tumor-avid radiopharmaceuticals to detect suggestive breast lesions and guide their stereotactic biopsy has some advantages over methods based on standard x-ray mammography. First, because the uptake mechanisms of most of the radiotracers used in nuclear oncology are related to the physiology of the tissue, some additional knowledge about the metabolic activity of the lesion can potentially be gained before biopsy. Furthermore, because the detection of suggestive breast lesions depends on metabolic differences between the tumor tissue and surrounding normal tissues, similarity in tissue densities between these tissue types should not significantly hinder the detection of these lesions with PEM.

The plots and results from fitting the data to straight lines, shown in Figure 4, indicate that our PEM-guided stereotactic method should be sufficiently accurate and precise for effective placement of biopsy needles or localization wires in most breast lesions detected with PEM. The potential advantage of using metabolic rather than density differences among tissue types to detect breast lesions and guide their biopsy is shown by a comparison of the images in Figure 5. The simulated lesion was not detected on the x-ray mammogram (Fig. 5A) but was detected on the PEM image (Fig. 5B). The results from the x-ray mammogram of the phantom were indeterminate because the density of the sphere and the density of the surrounding gelatin did not differ (much like a tumor in a radiographically dense breast). The sphere was successfully visualized with PEM, however, because of the difference between radiotracer concentration in the sphere and radiotracer concentration in the surrounding material (mimicking FDG-uptake differences between tumors and normal breast tissue). The detectability of breast lesions with FDG PEM depends, to a great extent, on lesion size and tumor-to-background radiotracer concentration. In a recent study, Raylman et al. (*15*) found that the PEM system they used could detect 10-mm-diameter simulated breast lesions in phantoms simulating the increased FDG uptake often observed in radiodense breasts (*16*). The tumor-to-background ratio in these successful tests ranged from 12.7:1 to 4.2:1.

The stereotactic biopsy technique successfully acquired samples from the simulated tumors in all 5 trials. These results show that this method has promise for reliably guiding the biopsy of suggestive breast tumors. Figure 6 shows that assessment of the needle position before firing was possible using this PEM system: the needle tip (shown in blue) is aligned with the simulated lesion, confirming that the needle will intercept the sphere when the gun is fired. In addition to allowing visual verification of needle position, the technique allows the stereotactic coordinates of the needle tip to be calculated and compared with the position previously calculated for the lesion. Although this method for verification of positioning proved successful, the use of a capillary tube containing FDG is not clinically suitable. Instead, a small, sealed point source containing the positron-emitting element $^{22}$Na (half-life, 2.6 y) can be mounted in the tip of the biopsy needle using a process developed by North American Scientific, Inc. (Chatsworth, CA). Hence, the tip of the needle itself will emit positrons and thus be detectable with PEM imagers.

## CONCLUSION

Our results confirmed the potential effectiveness of PEM for guiding the biopsy of suggestive breast lesions that preferentially accumulate FDG. PEM-guided biopsy should be most useful in situations in which PEM imaging is most effective—specifically, in women with breasts that are difficult to evaluate with x-ray mammography, such as cystic or radiographically dense breasts. Therefore, PEM and PEM-guided biopsy are intended not for the general population but for women in whom evaluation and diagnosis with standard methods is difficult. The ultimate usefulness of PEM-guided biopsy is linked to the effectiveness of PEM imagers in detecting suggestive breast lesions. Thus, research on improving the technique continues, including improvement of intrinsic resolution and correction of the effects of random and Compton scatter coincidence events. Finally, our encouraging results have led to the initiation of

a preclinical trial and the design of a dedicated PEM biopsy apparatus.

## ACKNOWLEDGMENTS

The authors thank Bryan Smith of the radiochemistry section of the Center for Advanced Imaging at West Virginia University for supplying the radionuclides used in this study and Lorie McCue of the Betty Puskar Breast Care Center of West Virginia University for acquiring the x-ray mammograms. This study was supported in part by a grant from West Virginia University and grant 1 R21 CA82752-01 from the National Cancer Institute.

## REFERENCES

1. Thompson CJ, Murthy K, Weinberg IN, Mako F. Feasibility of positron emission mammography. *Med Phys.* 1994;21:529–538.
2. Thompson CJ, Murthy K, Picard Y, Weinberg IN. Positron emission mammography (PEM): a promising technique for detecting breast cancer. *IEEE Trans Nucl Sci.* 1994;41:1012–1017.
3. Weinberg IN, Majewski S, Weisenberger AG, et al. Preliminary results for positron emission mammography: real-time functional breast imaging in a conventional mammographic gantry. *Eur J Nucl Med.* 1996;23:804–806.
4. Khalkhali I, Mishkin FS, Diggles LE, Klein SR. Radionuclide-guided stereotactic prebiopsy localization of nonpalpable breast lesions with normal mammograms. *J Nucl Med.* 1997;38:1019–1022.
5. Jackson VP, Hendrick RE, Feig SA, Kopans DB. Imaging of the radiographically dense breast. *Radiology.* 1993;188:297–301.
6. Kerlikowske K, Grady D, Barclay J, Sickles SA, Ernster V. Effect of age, breast density and family history on the sensitivity of first screening mammography. *JAMA.* 1996;276:33–38.
7. Grogan SK, Evans J, Cohen GP, MacMillen JH. Characteristics of breast carcinomas missed by screening radiologists. *Radiology.* 1997;204:131–135.
8. Lehman CD, White E, Peacock S, Drucker MJ, Urban N. Effect of age and breast density on screening mammograms with false-positive findings. *AJR.* 1999;173:1651–1655.
9. Raylman RR, Ficaro EP, Wahl RL. Stereotactic coordinates from ECT sinograms for radionuclide-guided biopsy. *J Nucl Med.* 1996;37:1562–1567.
10. Pani R, Soluri A, Pergola A, et al. Multi-PSPMT scintillating camera. *IEEE Trans Nucl Sci.* 1999;46:702–708.
11. Wojcik R, Majewski S, Steinbach D, Weisenberger AG. High spatial resolution gamma imaging detector based on 5′′ diameter R3292 hamamatsu PSPMT. *IEEE Trans Nucl Sci.* 1998;45:487–491.
12. Zasadny KR, Wahl RL. Standardized uptake values of normal tissues at PET with 2-[fluorine-18]-fluoro-2-deoxy-D-glucose: variations with body weight and a correction method. *Radiology.* 1993;189:847–850.
13. Avril N, Bense S, Ziegler SI, et al. Breast imaging with fluorine-18-FDG PET: quantitative image analysis. *J Nucl Med.* 1997;38:1186–1191.
14. Turkington TG, Williams NE, Hamblen SM, Coleman RE. Regional FDG uptake, attenuation, and geometries measurements for whole body phantom design [abstract]. *J Nucl Med.* 1999;40(suppl):281P.
15. Raylman RR, Majewski S, Wojcik R, et al. The potential role of positron emission mammography for detection of breast cancer: a phantom study. *Med Phys.* 2000;27:1943–1954.
16. Sugawara Y, Helvie MA, Zasadny KR, et al. Normal breast FDG uptake on PET versus body weight, age and mammographic density [abstract]. *J Nucl Med.* 1999:40(suppl):248P.